SKIN LESION EXTRACTION IN DERMOSCOPIC IMAGES BASED ON COLOUR ENHANCEMENT AND ITERATIVE SEGMENTATION

Gerald Schaefer [1], *Maher I. Rajab* [2], *M. Emre Celebi* [3] *and Hitoshi Iyatomi* [4]

[1]School of Engineering and Applied Science, Aston University, Birmingham, U.K.
[2]Department of Computer Engineering, Umm Al-Qura University, Makkah, Saudi Arabia
[3]Department of Computer Science, Louisiana State University, Shreveport, USA
[4]Department of Electrical Informatics, Hosei University, Tokyo, Japan

ABSTRACT

Accurate extraction of lesion borders is a crucial step in analysing dermoscopic skin lesion images. In this paper we present an effective approach to extracting lesion areas by combining an iterative segmentation algorithm with a pre-processing step that enhances colour information and image contrast. Following the pre-processing, analysis of the image background is conducted by iterative measurements based on median and standard deviation of non-lesion pixels, which in turn facilitates automatic and recurring noise reduction and enhancement. The algorithm does not depend on the use of rigid threshold values as an optimal thresholding algorithm is used to determine the optimal threshold iteratively. Extensive experimental evaluation is carried out on a dataset of 90 dermoscopy images with known ground truths obtained from three expert dermatologists. The results show that our approach is capable of providing good segmentation performance and that the colour enhancement step is indeed crucial as demonstrated by comparison with results obtained from the original RGB images.

Index Terms— medical imaging, skin cancer, dermoscopy, image segmentation, colour normalisation, contrast enhancement

1. INTRODUCTION

Malignant melanoma, the most deadly form of skin cancer, is one of the most rapidly increasing cancers in the world, with an estimated incidence of 62,480 and an estimated total of 8,420 deaths in the United States in 2008 alone [1]. Early diagnosis is particularly important since melanoma can be cured with a simple excision if detected early.

Dermoscopy has become one of the most important tools in the diagnosis of melanoma and other pigmented skin lesions. This non-invasive skin imaging technique involves optical magnification, which makes subsurface structures more easily visible when compared to conventional clinical images [2]. This in turn reduces screening errors and provides greater differentiation between difficult lesions such as pigmented Spitz nevi and small, clinically equivocal lesions [3]. However, it has also been demonstrated that dermoscopy may actually lower the diagnostic accuracy in the hands of inexperienced dermatologists [4]. Therefore, in order to minimise the diagnostic errors that result from the difficulty and subjectivity of visual interpretation, computerised image analysis techniques are highly sought after [5].

Automated border detection is often the first step in the automated analysis of dermoscopy images [6] and is crucial for two main reasons. First, the border structure provides important information for accurate diagnosis, as many clinical features, such as asymmetry, border irregularity, and abrupt border cutoff, are calculated directly from the border. Second, the extraction of other important clinical features such as atypical pigment networks, globules, and blue-white areas, critically depends on the accuracy of border detection.

Automated border detection is a challenging task since dermoscopy images often suffer from low contrast between the lesion and the surrounding skin. In addition, different images or even the same image but under different lighting conditions will lead to different image colours which can lead to reduced segmentation performance. In this paper we address these issues. We first pre-process the images using a colour normalisation technique [7] that both removes colour variations and enhances the contrast of the images. The processed images are then segmented using a technique that iteratively analyses the image background and derives an optimal threshold for segmentation. Results on a large set of dermoscopy lesion images confirm that our approach achieves good segmentation performance as judged based on manual borders obtained from three expert dermatologist. Our results also demonstrate that the colour normalisation step is indeed crucial in providing accurate segmentation.

The rest of the paper is organised as follows: In Section 2 we describe the colour normalisation technique that we employ as a pre-processing step. Section 3 details our iterative segmentation algorithm while experimental results are presented in Section 4. Section 5 concludes the paper.

2. COLOUR NORMALISATION AND CONTRAST ENHANCEMENT

In our approach we consider the problems of poor contrast and lack of colour calibration which are often encountered when analysing dermoscopy images. Different illumination or different devices will lead to different image colours [8] of the same lesion and hence to difficulties in the segmentation stage. Similarly, low contrast makes accurate border detection difficult [9]. We therefore address these issue by applying a colour normalisation technique, namely Automatic Color Equalization (ACE) [7], as a pre-processing step.

ACE colour normalisation is based on a model that is designed to merge two popular normalisation techniques, namely Grayworld [10] and MaxRGB [11] normalisation. Local adjustment is performed by considering the colour spatial distribution in the image.

ACE consists of two main stages: chromatic/spatial adjustment and dynamic tone reproduction scaling. The chromatic/spatial adjustment stage is the part where the actual colour normalisation is performed and the image contrast enhanced, while the second stage is responsible for accurate tone mapping and lightness constancy.

In detail, in the chromatic/spatial adjustment stage an intermediate image M is generated from an input image I according to

$$M_i(p) = \sum_{j, j \neq q} \frac{r(I_i(p) - I_i(j))}{d(p,q)}, \quad i = R, G, B \qquad (1)$$

where $I_i(p) - I_i(j)$ implements a lateral inhibition mechanism, $d(p,q)$ is the distance (in our experiments Euclidean distance) between pixel locations p and q and balances local and global filtering effects. q can be chosen to include the whole image or just a subset of it (we use the whole image). $r(.)$ is a function that accounts for the relative lightness of a pixel and was chosen to be a sloped saturation function with a slope of 5.

In the dynamic tone reproduction stage, the pixel values of the intermediate image M are transferred to generate the output image O. Various possibilities for this mapping are possible, and in our experiments we adopt a combined MaxRGB/Grayworld scaling that leads to

$$O_i(p) = 127.5 + s_i M_i(p), \quad i = R, G, B \qquad (2)$$

where s_i is the slope of the segment

$$[(min_p M_i(p), 0), (max_p M_i(p), 255)]$$

.

The effect of the employed colour normalisation is shown on an example in Figure 1 which displays a typical lesion image before and after the enhancement. Clearly, the processed version has a much better defined contrast which in turn should aid in deriving a better border detection.

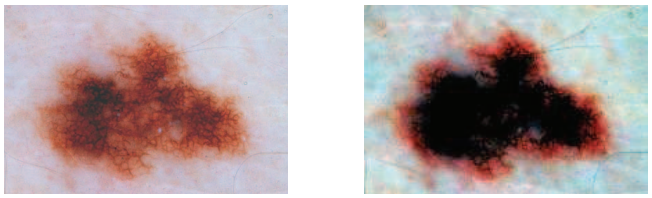

Fig. 1. Sample original lesion image (left) and the same image after colour normalisation (right).

3. ITERATIVE SKIN LESION SEGMENTATION

Two criteria are considered in the design of our proposed segmentation method: (1) an accurate search of the optimal lesion border can be achieved by analysing the whole image and consequently the true lesion border is also retrieved; approximation of the lesion border within the refined regions and curve fitting approaches are not adopted, (2) input parameters are mostly image dependent and have to be adjusted based on the properties of the class of images used in the segmentation method.

First, we apply a simple noise suppression method which aims to reduce artefacts such as hair that are often present in dermoscopic images. To do so, we subtract the median of the background followed by recursive Gaussian smoothing. To estimate the median of the background we inspect two strips (with width of 1/10 of the image width) located at the top and the bottom of the image and extract the median value of these regions.

Following noise reduction, we employ an iterative scheme to segment the image into regions containing the lesion and the background skin. To do so we apply an ISODATA algorithm to determine an optimal threshold value T for an image [12]. If I is the image and R_i denotes the i-th of N regions of the image, the iterative scheme for estimating the $N-1$ optimal thresholds and the N mean intensities are given by

$$T_{k+1} = \frac{\mu_{R_i,k} + \mu_{R_{i+1},k}}{2} \text{ until } T_{k+1} = T_k \qquad (3)$$

and

$$\mu_{R_i,k} = \frac{\sum_{m,n \in R_{i,k}} z(m,n)}{N_{R_i,k}} \qquad (4)$$

where T_{k+1} is the optimal threshold separating pixels in region R_i from pixels in region R_{i+1} and, at step k, $\mu_{R_i,k}$ represents the ratio of the mean pixel value $z(m,n)$ in region R_i to the total number of pixels $N_{R_i,k}$ in that region. The process is repeated based upon the newly generated threshold, until the threshold value has converged.

Finally, a post-processing step is applied that removes isolated pixels and small objects that are not likely to be part of the lesion.

4. EXPERIMENTAL RESULTS

We evaluated our approach on a large dataset of 90 dermoscopy images (23 invasive malignant melanoma and 67 benign) obtained from the EDRA Interactive Atlas of Dermoscopy [2], and the dermatology practices of Dr. Ashfaq Marghoob (New York, NY), Dr. Harold Rabinovitz (Plantation, FL) and Dr. Scott Menzies (Sydney, Australia). The benign lesions included nevocellular nevi and dysplastic nevi. Manual borders were obtained by selecting a number of points on the lesion border, connecting these points by a second-order B-spline and finally filling the resulting closed curve. Three sets of manual borders were determined by three expert dermatologists, Dr. William Stoecker, Dr. Joseph Malters, and Dr. James Grichnik using this method.

As performance measure we use the XOR measure proposed in [13] which quantifies the percentage border detection error by

$$\text{Error} = \frac{\text{Area}\,(AB \oplus MB)}{\text{Area}\,(MB)} \tag{5}$$

where AB and MB are the binary images obtained by filling the automatic and manual borders, respectively, $\oplus$ is the exclusive-OR (XOR) operation that gives the pixels for which AB and MB disagree, and Area(I) denotes the number of pixels in the binary image I.

The results for all 90 images as well as averages over the whole dataset are listed in Table 1. In there, we give the XOR measures obtained on each individual colour channel (i.e., red, green, and, blue) as well as on the luminance channel $L = (R+G+B)/3$ [14], averaged over all three ground truth segmentations. We do this both for unprocessed RGB images that only undergo the same segmentation method as detailed in Section 3 as well as our full algorithm that incorporates the colour normalisation step described in Section 2.

From Table 1 we can see that our approach is capable of achieving good segmentation performance which is characterised by an average XOR error of only 0.14 over the whole dataset when choosing the blue channel (as is often done in tumor segmentation [13]) or the green channel, respectively 0.18 for luminance L. This compares favourably to other lesion segmentation algorithms such as the orientation-sensitive fuzzy c-means algorithm [15] which produces an average error of 0.24 on the same dataset. We also see that the proposed application of a colour normalisation step proves crucial in achieving this performance as segmentation based on the same border detection algorithm but on unprocessed images is clearly inferior: results on the original RGB images show an average error of 0.25 for the blue channel respectively 0.39 based on luminance. An example of this difference is illustrated in Figure 2 which provides the final segmentations (based on the blue channel) of the two images from Figure 1 (which is Image 29 in Table 1). It is apparent that the segmentation obtained from the normalised image is more ac-

	RGB				ACE			
	R	G	B	L	R	G	B	L
1	0.74	0.47	0.33	0.51	0.29	0.21	0.14	0.21
2	1.06	1.06	0.40	0.84	0.54	0.20	0.11	0.28
3	1.09	0.43	0.24	0.59	0.40	0.17	0.11	0.23
4	1.07	1.07	1.07	1.07	0.36	0.10	0.07	0.18
5	0.47	0.24	0.17	0.30	0.19	0.15	0.10	0.14
6	1.09	0.74	0.33	0.72	0.25	0.12	0.07	0.15
7	1.14	0.76	0.30	0.73	0.26	0.16	0.12	0.18
8	1.18	1.18	1.18	1.18	0.21	0.08	0.06	0.11
9	1.08	0.65	1.08	0.94	0.10	0.07	0.06	0.08
10	1.23	1.22	0.52	0.99	0.09	0.12	0.17	0.13
11	0.60	0.38	0.28	0.42	0.37	0.09	0.07	0.17
12	0.48	0.21	0.18	0.29	0.23	0.13	0.11	0.16
13	0.41	0.25	0.19	0.28	0.28	0.25	0.19	0.24
14	0.47	0.28	0.20	0.31	0.16	0.12	0.12	0.13
15	0.40	0.19	0.16	0.25	0.17	0.09	0.09	0.12
16	0.65	0.35	0.28	0.42	0.42	0.10	0.12	0.21
17	0.23	0.10	0.06	0.13	0.07	0.05	0.05	0.05
18	0.36	0.28	0.24	0.29	0.15	0.08	0.09	0.11
19	0.28	0.21	0.17	0.22	0.17	0.16	0.13	0.16
20	0.32	0.17	0.12	0.20	0.19	0.12	0.10	0.14
21	0.39	0.22	0.16	0.26	0.30	0.19	0.15	0.21
22	0.38	0.22	0.15	0.25	0.27	0.15	0.11	0.18
23	0.40	0.29	0.20	0.30	0.25	0.10	0.09	0.15
24	0.40	0.20	0.12	0.24	0.20	0.06	0.06	0.11
25	0.79	0.52	0.41	0.57	0.67	0.30	0.25	0.41
26	0.43	0.28	0.18	0.30	0.30	0.17	0.13	0.20
27	0.63	0.33	0.21	0.39	0.29	0.11	0.11	0.17
28	0.37	0.23	0.15	0.25	0.24	0.18	0.13	0.18
29	0.51	0.22	0.15	0.29	0.36	0.13	0.11	0.20
30	0.52	0.27	0.20	0.33	0.32	0.18	0.14	0.21
31	0.34	0.19	0.13	0.22	0.24	0.16	0.11	0.17
32	0.26	0.15	0.11	0.17	0.11	0.10	0.17	0.13
33	0.23	0.10	0.07	0.13	0.13	0.06	0.05	0.08
34	0.23	0.11	0.07	0.14	0.07	0.07	0.12	0.09
35	0.34	0.19	0.11	0.21	0.21	0.08	0.07	0.12
36	0.30	0.15	0.10	0.18	0.11	0.04	0.04	0.07
37	0.73	0.24	0.19	0.38	0.30	0.08	0.08	0.15
38	0.36	0.20	0.15	0.24	0.15	0.16	0.18	0.17
39	0.29	0.13	0.09	0.17	0.06	0.07	0.08	0.07
40	0.46	0.23	0.16	0.29	0.30	0.11	0.08	0.16
41	0.25	0.12	0.09	0.15	0.08	0.07	0.11	0.08
42	0.41	0.23	0.16	0.27	0.23	0.09	0.08	0.13
43	0.50	0.24	0.19	0.31	0.32	0.22	0.20	0.25
44	0.31	0.14	0.09	0.18	0.05	0.06	0.06	0.05
45	0.27	0.09	0.06	0.14	0.11	0.07	0.05	0.08
46	0.77	0.45	0.27	0.50	0.33	0.30	0.32	0.32
47	1.04	0.58	0.43	0.68	0.28	0.23	0.23	0.25
48	0.17	0.08	0.12	0.12	0.09	0.15	0.16	0.13
49	0.19	0.12	0.23	0.18	0.09	0.11	0.20	0.13
50	0.63	0.35	0.22	0.40	0.42	0.16	0.11	0.23
51	0.57	0.32	0.25	0.38	0.39	0.14	0.13	0.22
52	0.23	0.17	0.17	0.19	0.06	0.08	0.12	0.09
53	0.32	0.19	0.11	0.21	0.17	0.10	0.07	0.12
54	0.30	0.19	0.19	0.22	0.12	0.09	0.08	0.10
55	0.07	0.08	0.14	0.09	0.05	0.04	0.09	0.06
56	0.14	0.15	0.16	0.15	0.06	0.08	0.11	0.08
57	0.56	0.37	0.28	0.40	0.38	0.19	0.14	0.24
58	0.39	0.21	0.14	0.25	0.26	0.14	0.10	0.17
59	0.28	0.20	0.12	0.20	0.13	0.08	0.06	0.09
60	0.37	0.26	0.20	0.28	0.18	0.19	0.29	0.22
61	0.32	0.19	0.14	0.22	0.18	0.10	0.16	0.15
62	0.49	0.33	0.31	0.38	0.34	0.22	0.25	0.27
63	0.57	0.23	0.16	0.32	0.45	0.11	0.07	0.21
64	0.30	0.21	0.18	0.23	0.11	0.09	0.09	0.09
65	0.29	0.16	0.10	0.18	0.10	0.11	0.16	0.12
66	0.52	0.27	0.20	0.33	0.14	0.15	0.25	0.18
67	0.70	0.30	0.23	0.41	0.32	0.09	0.07	0.16
68	0.43	0.22	0.27	0.31	0.29	0.36	0.48	0.38
69	0.81	0.29	0.15	0.42	0.25	0.07	0.13	0.15
70	0.43	0.17	0.12	0.24	0.14	0.05	0.11	0.10
71	1.02	0.48	0.41	0.64	0.25	0.08	0.08	0.14
72	0.50	0.31	0.31	0.37	0.40	0.18	0.29	0.29
73	0.55	0.26	0.21	0.34	0.33	0.13	0.10	0.18
74	0.93	0.59	0.48	0.66	0.64	0.20	0.20	0.35
75	0.82	0.43	0.28	0.51	0.26	0.21	0.18	0.22
76	0.76	0.58	0.46	0.60	0.32	0.13	0.10	0.18
77	0.66	0.32	0.24	0.41	0.23	0.09	0.17	0.16
78	0.68	0.38	0.30	0.45	0.14	0.09	0.09	0.11
79	0.73	0.43	0.18	0.45	0.45	0.29	0.21	0.32
80	0.40	0.27	0.22	0.30	0.21	0.09	0.08	0.13
81	0.58	0.32	0.26	0.38	0.35	0.27	0.43	0.35
82	0.87	0.59	0.49	0.65	0.50	0.23	0.15	0.29
83	0.92	0.67	0.48	0.69	0.25	0.14	0.14	0.18
84	0.98	0.16	0.11	0.42	0.93	0.11	0.07	0.37
85	1.09	0.95	0.56	0.87	0.16	0.06	0.08	0.10
86	1.19	1.11	0.82	1.04	0.49	0.19	0.16	0.28
87	0.62	0.36	0.24	0.40	0.22	0.16	0.12	0.16
88	0.51	0.10	0.07	0.23	0.16	0.06	0.05	0.09
89	0.77	0.48	0.34	0.53	0.27	0.12	0.10	0.16
90	0.95	0.40	0.35	0.57	0.67	0.55	0.80	0.67
average	0.57	0.34	0.25	0.39	0.26	0.14	0.14	0.18

Table 1. Experimental results of segmentation algorithm based on RGB and ACE input.

curate (average 0.36, 0.13, and 0.11 for segmentations based red, green, and blue channel) compared to that based on the original image (average errors of 0.51, 0.22, and 0.15).

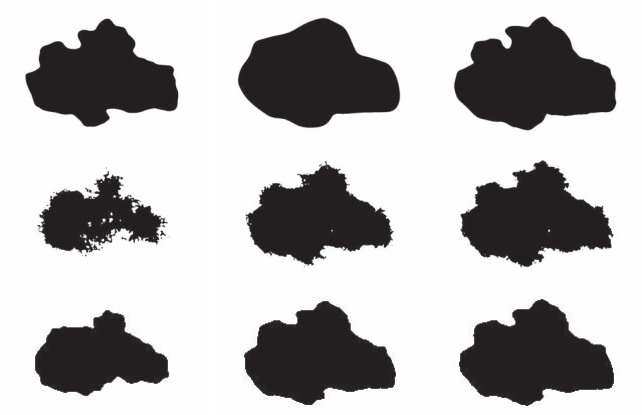

Fig. 2. Segmentation results for the images in Figure 1. Top row: manual segmentations derived by 3 dermatologists. Middle row: segmentation based on red, green, and blue channel of original lesion image. Bottom row: segmentation based on red, green, and blue channel of colour normalised image.

5. CONCLUSIONS

In this paper we have presented a successful approach to automatic identification of lesion borders in dermoscopic images. Importantly, we employ a colour normalisation technique to reduce colour variations and enhance image contrast. This is followed by a segmentation method that iteratively estimates threshold values for optimal separation of lesion and skin regions. Experiments on a large dataset of dermoscopy images have confirmed good segmentation accuracy as judged by comparison with manual borders obtained from three expert dermatologists, and have also demonstrated that the colour normalisation stage is crucial in achieving this performance.

References

[1] A. Jemal, R. Siegel, E. Ward, Y. Hao, J. Xu, T. Murray, and M.J. Thun, "Cancer statistics, 2008," *CA: A Cancer Journal for Clinicians*, vol. 58, no. 2, pp. 71–96, 2008.

[2] G. Argenziano, H.P. Soyer, and V. De Giorgi, *Dermoscopy: A Tutorial*, EDRA Medical Publishing & New Media, 2002.

[3] K. Steiner, M. Binder, M. Schemper, K. Wolff, and Pehamberger H., "Statistical evaluation of epiluminescence dermoscopy criteria for melanocytic pigmented lesions," *Journal of the American Academy of Dermatology*, vol. 29, no. 4, pp. 581–588, 1993.

[4] M. Binder, M. Schwarz, A. Winkler, A. Steiner, A. Kaider, K. Wolff, and H. Pehamberger, "Epiluminescence microscopy. a useful tool for the diagnosis of pigmented skin lesions for formally trained dermatologists," *Archives of Dermatology*, vol. 131, no. 3, pp. 286–291, 1995.

[5] M.G. Fleming, C. Steger, J. Zhang, J. Gao, A.B. Cognetta, I. Pollak, and C.R. Dyer, "Techniques for a structural analysis of dermatoscopic imagery," *Computerized Medical Imaging and Graphics*, vol. 22, no. 5, pp. 375–389, 1998.

[6] M.E. Celebi, H. Iyatomi, G. Schaefer, and W.V. Stoecker, "Lesion border detection in dermoscopy images," *Computerized Medical Imaging and Graphics*, vol. 33, no. 2, 2009.

[7] A. Rizzi, C. Gatta, and D. Marini, "A new algorithm for unsupervised global and local color correction," *Pattern Recognition Letters*, vol. 24, no. 11, pp. 1663–1677, July 2003.

[8] G. Finlayson and G. Schaefer, "Colour indexing across devices and viewing conditions," in *2nd International Workshop on Content-Based Multimedia Indexing*, 2001, pp. 215–221.

[9] D. Delgado, C. Butakoff, B.K. Ersboll, and W.V. Stoecker, "Independent histogram pursuit for segmentation of skin lesions," *IEEE Trans. Biomedical Engineering*, vol. 55, no. 1, pp. 157–161, 2008.

[10] G. Buchsbaum, "A spatial processor model for object colour perception," *Journal of the Franklin Institute*, vol. 310, pp. 1–26, 1980.

[11] E.H. Land, "The retinex theory of color constancy," *Scientific American*, pp. 108–129, 1977.

[12] T.W. Ridler and S. Calvard, "Picture thresholding using an iterative selection method," *IEEE Trans. Systems, Man and Cybernetics*, vol. 8, pp. 630–632, 1978.

[13] G.A. Hance, S.E. Umbaugh, R.H. Moss, and W.V. Stoecker, "Unsupervised color image segmentation with application to skin tumor borders," *IEEE Engineering in Medicine and Biology Magazine*, vol. 15, no. 1, pp. 104–111, 1996.

[14] Y. Ohta, T. Kanade, and T. Sakai, "Color information for region segmentation," *Computer Graphics Image Processing*, vol. 13, no. 3, pp. 222–241, July 1980.

[15] P. Schmid, "Segmentation of digitized dermatoscopic images by two-dimensional color clustering," *IEEE Trans. Medical Imaging*, vol. 18, no. 2, pp. 164–171, 1999.